

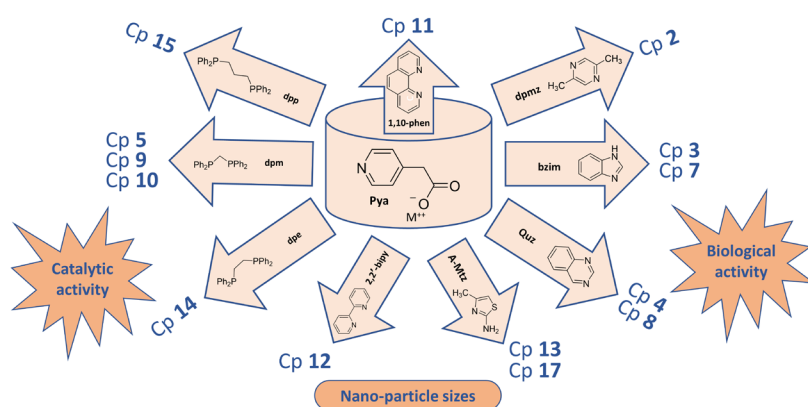
Full Paper | <http://dx.doi.org/10.17807/orbital.v13i1.1551>

# Nanosized Supramolecular Coordination Polymers Derived from Divalent Metal Ions, 4-Pyridylacetate and Auxiliary Ligands Containing Nitrogen and Phosphorus Donors

Aref A. M. Aly\* <sup>a</sup>, Asma I. El-Said <sup>a</sup>, Rasel A. Mukred <sup>b</sup>

A series of coordination polymers of Co(II), Ni(II), Cu(II) or Cd(II) comprising 4-pyridylacetate (pya) and certain auxiliary ligands including benzimidazole (Hbzim), 1,10-phenanthroline (phen), 2,2'-bipyridine (2,2'-bipy), 2-amino-4-methylthiazole (A-Mtz), quinazole (Quz), 2,5-dimethylpyrazine (dpmz), bis(diphenylphosphino)methane (dpm), 1,2-bis(diphenylphosphino)ethane (dpe) and 1,3-bis(diphenylphosphino) propane (dpp) were prepared and characterized by spectroscopic, magnetic and thermal techniques. In these coordination polymers 4-pyridylacetate coordinates to the metal ions in a monodentate fashion through the carboxylate oxygens and/or the pyridyl nitrogen. Octahedral structures around the metal ions were suggested for all the complexes. The kinetic analyses of the thermal decomposition of the complexes were studied using the Coats-Redfern equation. The kinetic and thermodynamic parameters of the thermal decomposition were also calculated and discussed. From the X-ray powder diffraction data, the crystal parameters as well as the particle sizes (15.7-18.7 nm) of the complexes could be evaluated. Some of the compounds exhibit catalytic activity. The biological activity of the compounds was screened as well.

## Graphical abstract



## Keywords

Nitrogen and phosphorus ligands  
4-Pyridylacetate  
Metal coordination polymers  
Spectroscopic investigations  
Thermal investigations

## Article history

Received 05 September 2020  
Revised 12 January 2021  
Accepted 12 January 2021  
Available online 26 March 2021

Editor: Jérôme Chauvin

## 1. Introduction

Crystal engineering of metal-organic coordination frameworks is currently one of the important subjects of

inorganic chemistry. This type of compounds usually provides network structures of fascinating properties [1–4]. It is known

<sup>a</sup> Chemistry Department., Faculty of Science, Assiut University, Egypt. <sup>b</sup> Department of Biology & Chemistry, College of Education, Al-Baida University, Yemen. \*Corresponding author. E-mail: [aref\\_20002001@yahoo.com](mailto:aref_20002001@yahoo.com)

that the incorporation of carboxylic acid groups into coordination compounds leads to the formation of fascinating supramolecular architectures besides some interesting properties [5,6]. 4-pyridylacetic acid is characterized by the existence of the methylene group between the pyridyl and the carboxylate terminal group that regulates the rigid/flexible nature of this ligand. Recent research work on its complexes suggest that these complexes possess a strong capability of forming interesting coordination polymer structures [7, 8]. The structure of 4-pyridylacetic acid is shown in Fig.1. Mixed ligand coordination polymers of 4-pyridylacetate are scarce in the literature [8]. Therefore, we embarked on the synthesis of a number of coordination polymers of 4-pyridylacetate including auxiliary ligands containing nitrogen and phosphorus donor atoms.

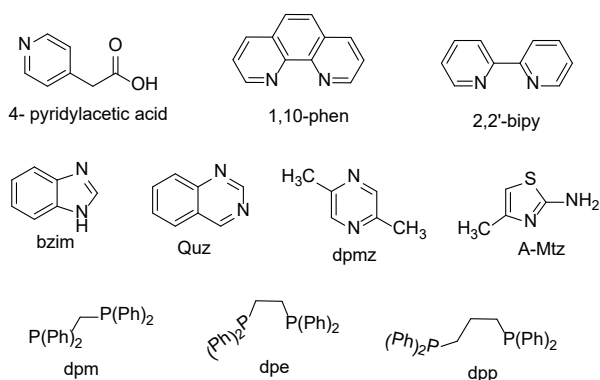


Fig. 1. Structure of the primary and secondary ligands.

## 2. Material and Methods

All chemicals were of analytical reagent grades. 2,2'-Bipyridine, quinazoline, 2-amino-4-methylthiazole, bis(diphenylphosphino)methane, 1,2-bis(diphenylphosphino)ethane and 1,3-bis(diphenylphosphino)propane were E. Merck grade. 4-Pyridylacetic acid (Hpya.HCl), 1,10-phenanthroline, benzimidazole and 2,5-dimethylpyrazine were Fluka grade. They were used without further purification.

### Physical measurements

Stoichiometric analysis (C, H, N, S) was performed using Analytischer Funktionstest Vario El Fab-Nr.11982027 elemental analyzer. The I.R spectra were recorded on a Shimadzu IR-470 spectrophotometer and the electronic spectra were obtained using a Shimadzu UV-2101 PC spectrophotometer. Thermal studies were carried out on a 2000 DuPont thermal analyzer at a heating rate of 10 °C min<sup>-1</sup>. Magnetic moments were measured at room temperature using magnetic susceptibility balance of type MSB-Auto. Molar susceptibilities were corrected for diamagnetism of the component atoms by the use of the Pascal's constants. The

calibrant used was Hg[Co(SCN)<sub>4</sub>]. The measurements of the kinetics of catalytic decomposition of hydrogen peroxide have been carried out using the gasometric approach. The X-ray powder diffractometer was a Philips 1700 version with H. TPW 1370/10, 4 KVA CuKαλ=1.54180 Å.

### Preparation of the coordination polymers

Coordination polymers of 4-pyridylacetate and the auxiliary ligands 1,10-phenanthroline, 2,2'-bipyridine, 2-amino-4-methylthiazole, quinazoline, 2,5-dimethylpyrazine, benzimidazole, bis(diphenylphosphine)methane, 1,2-bis(diphenylphosphino)ethane and 1,3-bis(diphenylphosphino)propane.

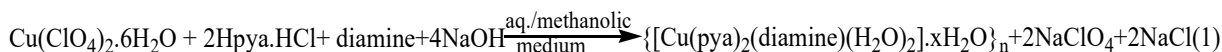
The pH value of an aqueous solution (5 mL) of Hpya.HCl (0.1 mmol) was adjusted to ca.6.5 by a dropwise addition of an aqueous solution of KOH (0.5 mmol). Transition metal ions solution (0.5 mmol) in MeOH (5 mL) was then carefully added to the above buffered solution with continuous stirring. Thereafter a solution of the respective secondary ligand (0.5 mmol) was added. The precipitated compounds were filtered off, washed using distilled water and methanol then dried over P<sub>2</sub>O<sub>5</sub> in a desiccator.

### Antibacterial activity test

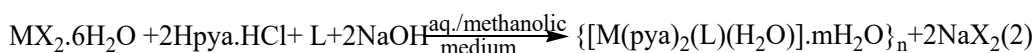
*In vitro* antibacterial activities of 4-pyridylacetate and some of its complexes were tested against a number of bacteria using the paper disc diffusion method [13]. The chosen strains were G(+) *Staphylococcus aureus*, *Bacillus cereus*, G(-) *Escherichia coli* and *Serratia marscence*. The nutrient agar and nutrient broth media were autoclaved for 20 min. at 121 °C and 15 lb pressure before inoculation. Then a suspension of the bacterial strains in nutrient broth medium was prepared after cooling in a test tube. From that suspension of bacterial strain 0.3 mL were taken in petri dishes where the nutrient agar was poured onto the plate and the petri dishes were shaken well and allowed to solidify. The test complexes dissolved in DMF were added dropwise to a 6 mm diameter filter paper disc placed at the center of each agar plate. The plates were then kept in an incubator at 37 °C. The width of the growth inhibition zone around the disc was measured after 24 h incubation.

## 3. Results and Discussion

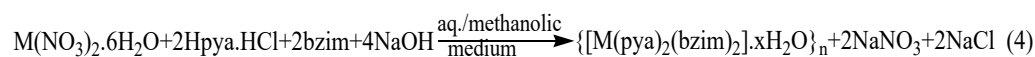
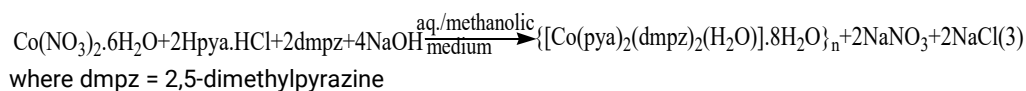
The complexes were prepared by the reaction of 4-pyridylacetic acid hydrochloride (Hpya.HCl) with different metal ions, namely Co(II), Ni(II) Cu(II) and Cd(II) and the secondary ligands 1,10-phenanthroline, 2,2'-bipyridine, 2-amino-4-methylthiazole, quinazoline, 2,5-dimethylpyrazine, benzimidazole, bis(diphenylphosphine)methane, 1,2-bis(diphenylphosphino)ethane and 1,3-bis(diphenylphosphino)propane at a pH ~ 6.5. The following equations (1- 7) represent formation of the complexes:



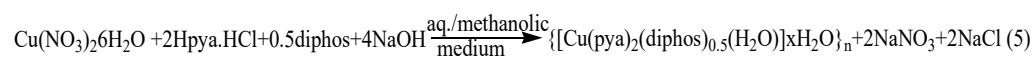
where diamine = 1,10-phenanthroline (phen) and 2,2'-bipyridine(2,2'-bipy), x= 2 or 6



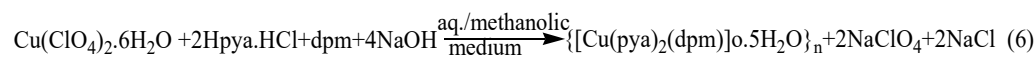
where M= Co(II), Ni(II), Cu(II) and Cd(II), X=NO<sub>3</sub> or Cl, m = 0.5-9 L = 2-amino-4-methylthiazole (A-Mtz) or quinazoline (Quz)



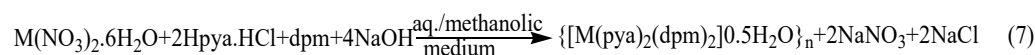
where M = Co(II) or Ni(II), x=2 or 5, bzim = benzimidazole



where diphos = 1,2-bis(diphenylphosphino)ethane or 1,3-bis(diphenylphosphino)propane x = 4 or 7



where dpm = bis (diphenylphosphino) methane (dpm)



where M = Co(II) or Ni(II).

**Table 1.** Color, molar conductance, elemental analysis, and decomposition point of the complexes **1-17**.

Complex	Color	$\Lambda_m (\Omega^{-1} \text{cm}^2 \text{mol}^{-1})$	Found (Calcd.%)				M.p., °C (Decomp.)
			C	H	N	S	
$\{[\text{Co}(\text{pya})_2(\text{H}_2\text{O})_2] \cdot \text{H}_2\text{O}\}_n$	1 Light pink	24	42.56 (43.42)	5.09 (5.22)	7.07 (7.26)	-	240
$\{[\text{Co}(\text{pya})_2(\text{dmpz})(\text{H}_2\text{O}) \cdot 8\text{H}_2\text{O}\}_n$	2 Light-brown	30	36.74 (36.26)	4.53 (5.79)	7.92 (8.46)	-	>360
$\{[\text{Co}(\text{pya})_2(\text{bzim})_2] \cdot 5\text{H}_2\text{O}\}_n$	3 violet	29	50.94 (50.98)	4.62 (5.51)	13.48 (12.74)	-	>360
$\{[\text{Co}(\text{pya})_2(\text{Quz})(\text{H}_2\text{O})] \cdot 1.5\text{H}_2\text{O}\}_n$	4 brown	25	42.30 (41.93)	6.83 (5.54)	9.35 (8.90)	-	>360
$\{[\text{Co}(\text{pya})_2(\text{dpm})_2] \cdot 0.5\text{H}_2\text{O}\}_n$	5 Light pink	34	70.21 (69.18)	5.24 (5.27)	2.35 (2.52)	-	310
$\{[\text{Ni}(\text{pya})_2(\text{H}_2\text{O})_2] \cdot \text{H}_2\text{O}\}_n$	6 Light -blue	27	44.76 (45.56)	4.83 (4.92)	7.25 (7.59)	-	285
$\{[\text{Ni}(\text{pya})_2(\text{bzim})_2] \cdot 2\text{H}_2\text{O}\}_n$	7 Light- violet	35	55.91 (55.56)	6.31 (5.01)	12.93 (13.88)	-	>360
$\{[\text{Ni}(\text{pya})_2(\text{Quz})(\text{H}_2\text{O})] \cdot 1.5\text{H}_2\text{O}\}_n$	8 Light-brown	23	52.78 (53.90)	4.41 (4.7)	11.92 (11.43)	-	>360
$\{[\text{Ni}(\text{pya})_2(\text{dpm})_2] \cdot 0.5\text{H}_2\text{O}\}_n$	9 Light brown	31	70.22 (69.10)	5.24 (5.27)	2.36 (2.52)	-	315
$\{[\text{Cu}(\text{pya})_2(\text{H}_2\text{O})_2]\}_n$ Ref[40]	10 -	-	-	-	-	-	-
$\{[\text{Cu}(\text{pya})_2(\text{phen})(\text{H}_2\text{O})_2] \cdot 2\text{H}_2\text{O}\}_n$	11 Greenish-blue	40	50.37 (50.92)	3.76 (3.18)	9.93 (9.58)	-	305
$\{[\text{Cu}(\text{pya})_2(2,2'\text{-bipy})(\text{H}_2\text{O})_2] \cdot 6\text{H}_2\text{O}\}_n$	12 Dark- blue	42	44.83 (45.17)	5.30 (5.69)	9.80 (8.80)	-	310
$\{[\text{Cu}(\text{pya})_2(\text{A-Mtz})(\text{H}_2\text{O})] \cdot 9\text{H}_2\text{O}\}_n$	13 Blue	32	33.24 (34.20)	5.75 (4.36)	8.86 (7.80)	5.07 (3.87)	320
$\{[\text{Cu}(\text{pya})_2(\text{dpe})_{0.5}(\text{H}_2\text{O})] \cdot 7\text{H}_2\text{O}\}_n$	14 Blue	22	48.62 (47.6)	5.06 (5.06)	3.21 (4.11)	-	240
$\{[\text{Cu}(\text{pya})_2(\text{dpp})_{0.5}(\text{H}_2\text{O})] \cdot 4\text{H}_2\text{O}\}_n$	15 Blue	24	51.81 (51.87)	4.79 (5.54)	3.55 (4.39)	-	230
$\{[\text{Cu}(\text{pya})_2(\text{dpm})] \cdot 0.5\text{H}_2\text{O}\}_n$	16 Light blue	24	62.39 (64.05)	4.89 (4.83)	2.39 (3.83)	-	280
$\{[\text{Cd}(\text{pya})_2(\text{A-Mtz})(\text{H}_2\text{O})] \cdot 2\text{H}_2\text{O}\}_n$	17 White	28	38.96 (39.73)	4.74 (5.50)	10.09 (9.71)	5.77 (5.20)	330

The composition of the complexes was justified by elemental analysis (Table 1). The complexes are air stable and do not dissolve in common organic solvents, except in DMSO or DMF. Molar conductivity of the prepared coordination polymers was measured at a concentration of  $10^{-3}$  M in dimethyl sulfoxide (DMSO). The conductivity values indicate the non-electrolyte nature of the compounds [9] ( $22-42 \Omega^{-1} \text{cm}^2 \text{mol}^{-1}$ ).

### IR Spectra

The infrared spectra of the complexes **1-17** exhibit characteristic features of pyridine bearing carboxylate substituents. The complexes show bands in the range 1600-

1563  $\text{cm}^{-1}$  attributed to the asymmetric stretching vibrations and those in the range 1440-1380  $\text{cm}^{-1}$  are ascribed to the symmetric stretching vibrations of the carboxylate groups. The  $\Delta\nu$  values ( $\nu_{\text{as}}-\nu_{\text{s}}$ ) (200-143)  $\text{cm}^{-1}$  are typical of monodentate carboxylates [10]. The IR spectra of complexes **1-17** show further the stretching vibration  $\nu_{(\text{C}=\text{N})}$  for pyridyl rings in the 1600-1450  $\text{cm}^{-1}$  region [11]. The IR spectra of the complexes **2-4, 7, 8, 11** and **12** exhibit characteristic vibrations of  $\nu_{(\text{C}=\text{N})}$  for benzimidazole, o-phenanthroline, 2,2'-bipyridine, quinazoline, 2,5-dimethylpyrazine in the range 1590-1430  $\text{cm}^{-1}$  [12-14].

The stretching vibrations of  $\text{NH}_2$  in the complexes **13** and **17** for 2-amino-4-methylthiazole occur in the range 3400-3200  $\text{cm}^{-1}$  [15].

Coordination of the phosphines in the complexes **5**, **9**, **14**, **15** and **16** is indicated from the appearance of a band at 770-695  $\text{cm}^{-1}$  associated with the PhP- moiety [16].

The stretching vibration of  $\nu_{\text{H}_2\text{O}}$  of lattice water is assigned to the bands in the region 3500-3050  $\text{cm}^{-1}$ . The

stretching vibration of coordinated water is located in the region 3350-2800  $\text{cm}^{-1}$  [15]. The  $\nu(\text{M-N})$  and  $\nu(\text{M-O})$  vibrations in all the complexes are manifested by the appearance of a band in 428-410  $\text{cm}^{-1}$  and 520-440  $\text{cm}^{-1}$  regions, respectively. The main spectral bands of 4-pyridylacetate ternary complexes are recorded in Table 2.

**Table 2.** IR spectral data of the complexes **1-17**.

Complex	$\nu_{\text{as}(\text{COO})}$	$\nu_{\text{s}(\text{COO})}$	$\Delta\nu$	$\nu(\text{C=N})$	$\nu(\text{M-O})$	$\nu(\text{M-N})$	$\nu(\text{pph}_2+\text{p.cH}_2)$	$\nu_{\text{H}_2\text{O coord-}}$	$\nu_{\text{H}_2\text{O Lattice}}$	
$\{\text{Co}(\text{pya})_2(\text{H}_2\text{O})_2\}_n$	<b>1</b>	1563	1420	143	-	520	420	-	3150	3400
$\{\text{Co}(\text{pya})_2(\text{dmpz})(\text{H}_2\text{O}) \cdot 8\text{H}_2\text{O}\}_n$	<b>2</b>	1590	1410	180	1540	450	410	-	2900	3350
$\{\text{Co}(\text{pya})_2(\text{bzim})_2\}_n$	<b>3</b>	1575	1420	155	1500	480	425	-	2900	3350
$\{\text{Co}(\text{pya})_2(\text{Quz})(\text{H}_2\text{O})\}_n$	<b>4</b>	1580	1380	200	1575	480	420	-	-	3350
$\{\text{Co}(\text{pya})_2(\text{dpm})_2\}_n$	<b>5</b>	1580	1425	155	-	500	410	740	-	-
$\{\text{Ni}(\text{pya})_2(\text{H}_2\text{O})_2\}_n$	<b>6</b>	1570	1420	150	-	480	420	-	2850	3320
$\{\text{Ni}(\text{pya})_2(\text{bzim})_2\}_n$	<b>7</b>	1590	1430	160	1550	440	400	-	-	3100
$\{\text{Ni}(\text{pya})_2(\text{Quz})(\text{H}_2\text{O})\}_n$	<b>8</b>	1575	1380	195	1575	480	400	-	3050	3400
$\{\text{Ni}(\text{pya})_2(\text{dpm})_2\}_n$	<b>9</b>	1580	1425	155	-	495	410	700	-	3450
$\{\text{Cu}(\text{pya})_2(\text{H}_2\text{O})_2\}_n$ Ref[40]	<b>10</b>	1583	1425	158	-	510	420	-	3120	3420
$\{\text{Cu}(\text{pya})_2(\text{phen})(\text{H}_2\text{O})_2\}_n$	<b>11</b>	1580	1420	160	1520	490	420	-	3350	3500
$\{\text{Cu}(\text{pya})_2(2,2'\text{-bipy})(\text{H}_2\text{O})_2\}_n$	<b>12</b>	1600	1440	160	1490	510	428	-	3100	3600
$\{\text{Cu}(\text{pya})_2(\text{A-Mtz})(\text{H}_2\text{O})\}_n$	<b>13</b>	1580	1390	190	-	480	410	-	2350	3600
$\{\text{Cu}(\text{pya})_2(\text{dpe})_{0.5}(\text{H}_2\text{O})\}_n$	<b>14</b>	1580	1425	155	-	500	420	700	2900	-
$\{\text{Cu}(\text{pya})_2(\text{dpp})_{0.5}(\text{H}_2\text{O})\}_n$	<b>15</b>	1583	1410	173	-	500	420	740	3150	-
$\{\text{Cu}(\text{pya})_2(\text{dpm})_{0.5}(\text{H}_2\text{O})\}_n$	<b>16</b>	1575	1390	185	-	480	510	700	-	-
$\{\text{Cd}(\text{pya})_2(\text{A-Mtz})(\text{H}_2\text{O})\}_n$	<b>17</b>	1585	1420	165	-	480	410	740	-	3550

### UV-Vis spectra and magnetic susceptibility measurement

The electronic spectral data of the coordination polymers were recorded in DMSO in Table 3. All the coordination polymers exhibit a band in the region 300-342 nm attributed to the  $n \rightarrow \pi^*$  transition and a band in the region 260-287 nm is ascribed to the  $\pi \rightarrow \pi^*$  transition, while the bands observed in the region 350-450 nm for complexes **1-3**, **6-8**, **15** and **17** are assigned to an intraligand charge transfer transition (IL-charge transfer).

The cobalt(II) coordination polymers **1-5** display magnetic moment values in the range 3.8-4.8 B.M consistent with an octahedral environment around  $\text{Co(II)}$ , typical for high spin  $d^7$  system with three unpaired electrons. Correspondingly a band appears at 550-600 nm attributed to the  ${}^1\text{A}_{1g} \rightarrow {}^1\text{T}_{2g}$  transition.

In case of the Ni(II) coordination polymers **6-9** the magnetic moments were found in the range 3.7-3.2 B.M, as predicted for octahedral high spin  $d^8$  system with two unpaired electrons. They display a band in the region 625-700 nm assigned to the transition  ${}^3\text{A}_{2g} \rightarrow {}^3\text{T}_{1g}(\text{F})$ .

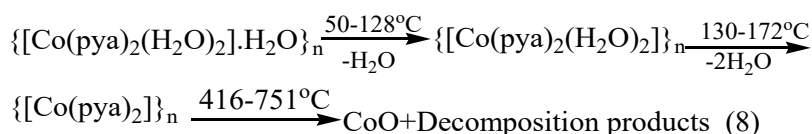
The electronic spectra of the Cu(II) coordination polymers **10-13** show a band in the range 700-851 nm which may be assigned to the  ${}^2\text{E}_g \rightarrow {}^2\text{T}_{2g}$  transition indicating octahedral geometry around  $\text{Cu(II)}$ , which is supported by its magnetic moment value in the range 1.7-1.6 B.M. Though three transitions are expected in this case, they are close in energy and often appear in the form of one broad band envelop. The electronic spectra for the copper (II) complexes **14-15** exhibits a weak-band centered at 860-878 nm, which corresponding to the  ${}^2\text{B}_{1g} \rightarrow {}^2\text{A}_{1g}$  transition in square planar geometries. Band assignment was made according to literature assignments for compounds of similar geometries [17].

The suggested structures based on the above discussed spectral and magnetic data for the 4-pyridylacetate complexes are shown in figures 2-4.

### Thermal decomposition of the complexes

Thermogravimetric (TG) and differential thermogravimetric (DTA) analysis were carried out for 4-pyridylacetate coordination polymers from ambient temperature to 750  $^{\circ}\text{C}$ . The decomposition steps of the complexes were discussed in terms of the proposed formula of the complexes. The thermal decomposition was carried out in dynamic air. The thermal decomposition of compounds **1** and **16** were selected to be described in detail.

The decomposition of the coordination polymer  $\{\text{Co}(\text{pya})_2(\text{H}_2\text{O})_2\}_n$  **1** proceeds in four steps (Fig. 6). The mass loss during the first step (50-128  $^{\circ}\text{C}$ ) is due to the release of one lattice water molecule (calc. 4.8 %, found 4.6%). The DTG curve displays correspondingly a peak at 108  $^{\circ}\text{C}$  while the DTA curve furnishes an endothermic peak at 111  $^{\circ}\text{C}$ . The second step (130-172  $^{\circ}\text{C}$ ) is related to detachment of the two coordinated water molecules (calc. 9.3 %, found 10.6 %). This step gives a DTG midpoint at 160  $^{\circ}\text{C}$  and an endothermic effect at 161  $^{\circ}\text{C}$  in the DTA curve. The third step (174-308  $^{\circ}\text{C}$ ) (40.0 %), produces a DTG midpoint at 243  $^{\circ}\text{C}$  and an exothermic effect at 245  $^{\circ}\text{C}$  in the DTA curve. The fourth step (22.3 %) is in fact composed of a number of overlapped steps (388-460  $^{\circ}\text{C}$ ). The DTG midpoint occurs at 429  $^{\circ}\text{C}$  that is associated with an exothermic peak at 432  $^{\circ}\text{C}$ . The final stable residue is identified from the mass loss consideration to be  $\text{CoO}$  (calc. 19.3 %, found 19.4 %) (Equation 8).

**Table 3.** Electronic spectral data of the complexes 1-17 (nm).

Complex		$\lambda_{\text{max}}$ (nm)	Assignment	$\mu_{\text{eff}}(\text{B.M})$
$\{[\text{Co}(\text{pya})_2(\text{H}_2\text{O})_2] \cdot \text{H}_2\text{O}\}_n$	1	550	$^4\text{T}_{1g} \rightarrow ^4\text{T}_{2g}$	4.2
		400	charge transfer	
		340	$n \rightarrow \pi^*$	
		280	$\pi \rightarrow \pi^*$	
$\{[\text{Co}(\text{pya})_2(\text{dmpz})(\text{H}_2\text{O}) \cdot 8\text{H}_2\text{O}\}_n$	2	555	$^4\text{T}_{1g} \rightarrow ^4\text{T}_{2g}$	3.8
		379	charge transfer	
		300	$n \rightarrow \pi^*$	
		280	$\pi \rightarrow \pi$	
$\{[\text{Co}(\text{pya})_2(\text{bzim})_2] \cdot 5\text{H}_2\text{O}\}_n$	3	600	$^4\text{T}_{1g} \rightarrow ^4\text{T}_{2g}$	3.9
		380	charge transfer	
		320	$n \rightarrow \pi^*$	
		280	$\pi \rightarrow \pi$	
$\{[\text{Co}(\text{pya})_2(\text{Quz})(\text{H}_2\text{O})] \cdot 1.5\text{H}_2\text{O}\}_n$	4	559	$^4\text{T}_{1g} \rightarrow ^4\text{T}_{2g} (u_1)$	3.9
		339	$n \rightarrow \pi^*$	
		280	$\pi \rightarrow \pi$	
		550	$^4\text{T}_{1g} \rightarrow ^4\text{T}_{2g} (u_1)$	
$\{[\text{Co}(\text{pya})_2(\text{dpm})_2] \cdot 0.5\text{H}_2\text{O}\}_n$	5	340	$n \rightarrow \pi^*$	4.8
		280	$\pi \rightarrow \pi$	
		625	$^3\text{A}_{2g} \rightarrow ^3\text{T}_{1g}$	
		370	$n \rightarrow \pi^*$	
$\{[\text{Ni}(\text{pya})_2(\text{H}_2\text{O})_2] \cdot \text{H}_2\text{O}\}_n$	6	270	$\pi \rightarrow \pi$	3.2
		700	$^3\text{A}_{2g} \rightarrow ^3\text{T}_{1g}$	
		450	$n \rightarrow \pi^*$	
		280	$\pi \rightarrow \pi$	
$\{[\text{Ni}(\text{pya})_2(\text{bzim})_2] \cdot 2\text{H}_2\text{O}\}_n$	7	635	$^3\text{A}_{2g} \rightarrow ^3\text{T}_{1g}$	3.7
		360	$n \rightarrow \pi^*$	
		287	$\pi \rightarrow \pi$	
		625	$^3\text{A}_{2g} \rightarrow ^3\text{T}_{1g}$	
$\{[\text{Ni}(\text{pya})_2(\text{dpm})_2] \cdot 0.5\text{H}_2\text{O}\}_n$	9	310	$n \rightarrow \pi^*$	3.4
		260	$\pi \rightarrow \pi$	
		700	$^2\text{E}_g \rightarrow ^2\text{T}_{2g}$	
		305	$n \rightarrow \pi^*$	
$\{[\text{Cu}(\text{pya})_2(\text{H}_2\text{O})_2]\}_n$ Ref[40]	10	260	$\pi \rightarrow \pi$	1.6
		750	$^2\text{E}_g \rightarrow ^2\text{T}_{2g}$	
		310	$n \rightarrow \pi^*$	
		280	$\pi \rightarrow \pi$	
$\{[\text{Cu}(\text{pya})_2(\text{phen})(\text{H}_2\text{O})_2] \cdot 2\text{H}_2\text{O}\}_n$	11	700	$^2\text{E}_g \rightarrow ^2\text{T}_{2g}$	1.7
		340	$n \rightarrow \pi^*$	
		280	$\pi \rightarrow \pi$	
		860	$^2\text{B}_{1g} \rightarrow ^2\text{A}_{1g}$	
$\{[\text{Cu}(\text{pya})_2(2,2'\text{-bipy})(\text{H}_2\text{O})_2] \cdot 6\text{H}_2\text{O}\}_n$	12	340	$n \rightarrow \pi^*$	1.7
		280	$\pi \rightarrow \pi$	
		851	$^2\text{E}_g \rightarrow ^2\text{T}_{2g}$	
		330	$n \rightarrow \pi^*$	
$\{[\text{Cu}(\text{pya})_2(\text{A-Mtz})(\text{H}_2\text{O})] \cdot 9\text{H}_2\text{O}\}_n$	13	270	$\pi \rightarrow \pi$	1.7
		878	$^2\text{B}_{1g} \rightarrow ^2\text{A}_{1g}$	
		330	$n \rightarrow \pi^*$	
		275	$\pi \rightarrow \pi^*$	
$\{[\text{Cu}(\text{pya})_2(\text{dpe})_{0.5}(\text{H}_2\text{O})] \cdot 7\text{H}_2\text{O}\}_n$	14	860	$^2\text{B}_{1g} \rightarrow ^2\text{A}_{1g}$	1.8
		350	$n \rightarrow \pi^*$	
		275	$\pi \rightarrow \pi$	
		860	$^2\text{B}_{1g} \rightarrow ^2\text{A}_{1g}$	
$\{[\text{Cu}(\text{pya})_2(\text{dpp})_{0.5}(\text{H}_2\text{O})] \cdot 4\text{H}_2\text{O}\}_n$	15	342	$n \rightarrow \pi^*$	1.6
		275	$\pi \rightarrow \pi$	
		860	$^2\text{B}_{1g} \rightarrow ^2\text{A}_{1g}$	
		342	$n \rightarrow \pi^*$	
$\{[\text{Cu}(\text{pya})_2(\text{dpm})] \cdot 0.5\text{H}_2\text{O}\}_n$	16	275	$\pi \rightarrow \pi$	1.7
		350	$n \rightarrow \pi^*$	
		265	$\pi \rightarrow \pi$	
		350	$n \rightarrow \pi^*$	
$\{[\text{Cd}(\text{pya})_2(\text{A-Mtz})(\text{H}_2\text{O})] \cdot 2\text{H}_2\text{O}\}_n$	17	265	$\pi \rightarrow \pi$	-

The stepwise decomposition of the complex  $\{[\text{Cu}(\text{pya})_2(\text{dpm})] \cdot 0.5\text{H}_2\text{O}\}_n$  **16** (Fig. 7) is characterized by four steps in the temperature ranges 40-256, 258-380, 381-503, and 504-553 °C. The first step accounts for the detachment of the half lattice water molecule (calc. 1.2%, found 1.0%). The DTG curve shows this thermal event at 120 °C (endothermic effect in the DTA curve at 121 °C). The second step is composed of three overlapping steps (28.2 %). The DTG curve exhibits three midpoints at 285, 342 and 372 °C with three

exothermic peaks in the DTA curve at 298, 324 and 375 °C, respectively. The third stage composed of three overlapping steps (21.4 %). This step has three DTG midpoints appearing at 412, 437 and 491 °C and three endothermic peaks in the DTA curve at 413, 438 and 503 °C. The fourth step of mass loss 7.6% possesses a DTG midpoint at 528 °C and an exotherm at 531 °C. Thereafter a continues decomposition sets in without conclusive information (Equation 9).

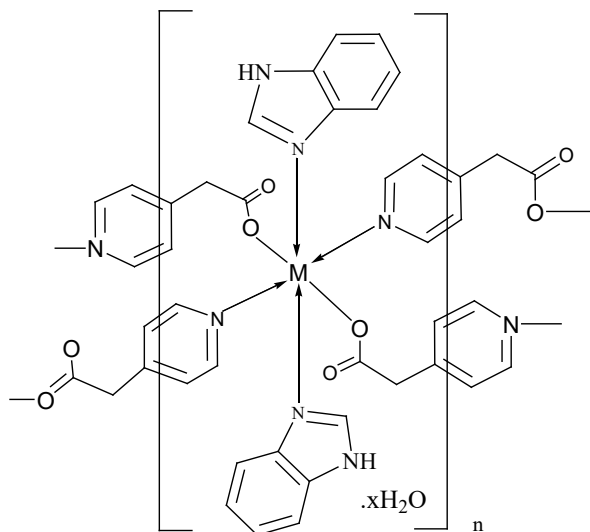
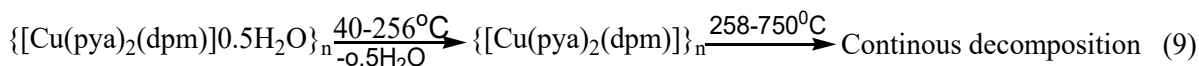


Fig. 2. Suggested structure of  $\{[\text{M}(\text{py})_2(\text{bzim})_2]x\text{H}_2\text{O}\}_n$ . Where  $\text{M} = \text{Co}(\text{II})$  or  $\text{Ni}(\text{II})$ ,  $x=5$  or  $2$ .

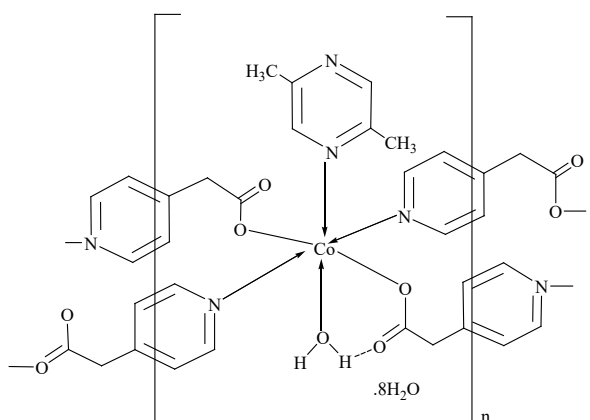


Fig. 3. Suggested structure of  $\{[\text{Co}(\text{py})_2(\text{dmpz})(\text{H}_2\text{O})] \cdot 8\text{H}_2\text{O}\}_n$ .

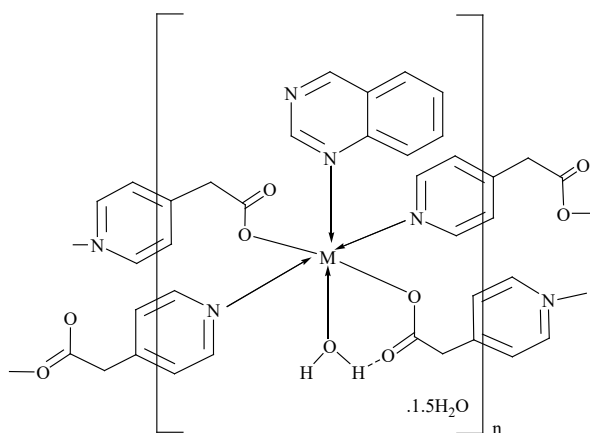


Fig. 4. Suggested structure of  $\{[\text{M}(\text{py})_2(\text{Quz})(\text{H}_2\text{O})] \cdot 1.5\text{H}_2\text{O}\}_n$ . Where  $\text{M} = \text{Co}(\text{II})$  or  $\text{Ni}(\text{II})$ .

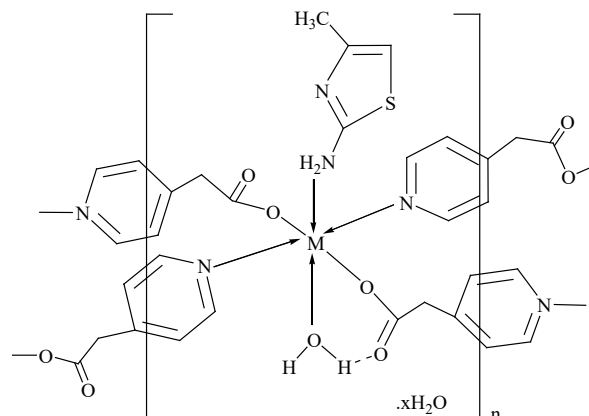


Fig. 5. Suggested structure of  $\{[\text{M}(\text{py})_2(\text{A-Mtz})(\text{H}_2\text{O})] \cdot x\text{H}_2\text{O}\}_n$ . Where  $\text{M} = \text{Cu}(\text{II})$  and  $\text{Cd}(\text{II})$ ,  $x = 9$  or  $2$ .

### Kinetic Analysis parameters

The kinetic parameters such as activation energy ( $E^*$ ) and pre-exponential factor ( $Z$ ) and ( $n$ ) order of the decomposition reactions were evaluated graphically by employing the Coats–Redfern [18] equation.

### The Coats-Redfern equation

$$\ln[1-(1-\alpha)^{1-n} / (1-n)T^2] = M / T + B \quad \text{for } n \neq 1 \quad (10)$$

$$\ln[-\ln(1-\alpha) / T^2] = M / T + B \quad \text{for } n = 1 \quad (11)$$

where  $\alpha$  is the fraction of material decomposed,  $n$  is the order of the decomposition reaction and  $M = E^*/R$  and  $B = ZR/\Phi E$ ;  $E$ ,  $R$ ,  $Z$  and  $\Phi$  are the activation energy, gas constant, pre-exponential factor and heating rate, respectively.

The correlation coefficient  $r$  is computed using the least squares method for equations (10) and (11). Linear curves were drawn for different values of  $n$  ranging from 0 to 2. The value of  $n$ , which gave the best fit, was chosen as the order parameter for the decomposition stage of interest. The kinetic parameters were calculated from the plots of the left hand side of equations (10) and (11) against  $1/T$ .

The kinetic parameters of decomposition process of the complexes, namely activation energy ( $E^*$ ), order ( $n$ ) of the decomposition reaction and the pre-exponential factor ( $Z$ ) are evaluated graphically by using the Coats–Redfern equation shown in Fig. 11.

The thermodynamic parameters, namely the activation enthalpy ( $\Delta H^*$ ), the activation entropy ( $\Delta S^*$ ), and the free energy of activation ( $\Delta G^*$ ) were calculated using the following equations:

$$\Delta S^* = 2.303 [\log(Zh/kT)]R \quad (12)$$

$$\Delta H^* = E^* - RT \quad (13)$$

$$\Delta G^* = \Delta H^* - T_s \Delta S^* \quad (14)$$

where  $Z$ ,  $k$ , and  $h$  are the pre-exponential factor, Boltzman, and Plank constants, respectively. The values are summarized in Table 4.

The negative  $\Delta S^*$  values of the first decomposition step of the complexes suggest that the activated complex is more

ordered than the reactants due to polarization of bonds in the activated state and that the reactions are slower than normal thus leading to stable compounds. This may indicate that

these decomposition reactions are non-spontaneous, a fact that is further substantiated by the positive values of  $\Delta G^*$  [19, 20].

**Table 4.** Thermal decomposition data of the complexes in dynamic air.

Complex	Step	TG/DTG			Mass loss (%)
		Ti/°C	Tm/°C	Tf/°C	
{[Co(pyra) <sub>2</sub> (H <sub>2</sub> O) <sub>2</sub> ].H <sub>2</sub> O} <sub>n</sub>	1 <sup>st</sup>	50	108	128	4.60
	2 <sup>nd</sup>	130	160	172	10.6
	3 <sup>rd</sup>	174	243	308	40.0
	4 <sup>th</sup>	388	429	460	22.3
{[Co(pyra) <sub>2</sub> (Quz)(H <sub>2</sub> O)]1.5H <sub>2</sub> O} <sub>n</sub>	1 <sup>st</sup>	42	66	102	7.10
	2 <sup>nd</sup>	104	360	381	68.6
{[Ni(pyra) <sub>2</sub> (H <sub>2</sub> O) <sub>2</sub> ].H <sub>2</sub> O} <sub>n</sub>	1 <sup>st</sup>	45	51	158	4.2
	2 <sup>nd</sup>	160	174	186	8.5
	3 <sup>rd</sup>	310	262	400	42.9
	4 <sup>th</sup>	401	393	751	23.0
{[Cu(pyra) <sub>2</sub> (H <sub>2</sub> O) <sub>2</sub> ] <sub>n</sub>	1 <sup>st</sup>	62	88	116	9.6
	2 <sup>nd</sup>	120	193	224	28.8
	3 <sup>rd</sup>	226	230	244	11.8
	4 <sup>th</sup>	246	296	280	13.3
	5 <sup>th</sup>	282	300	751	14.8
{[Cu(pyra) <sub>2</sub> (dpm)].0.5H <sub>2</sub> O} <sub>n</sub>	1 <sup>st</sup>	40	120	256	1.0
	2 <sup>nd</sup>	258	342	380	28.2
	3 <sup>rd</sup>	381	412	503	21.4
	4 <sup>th</sup>	504	528	553	7.60

T<sub>i</sub> = Initial temperature & T<sub>m</sub> = Maximum temperature & T<sub>f</sub> = Final temperature.

**Table 5.** Kinetic and thermodynamic parameters of the complexes in dynamic air.

Complex	Step	Parameters						
		r	n	$\Delta E^*$	Z	$\Delta H^*$	$\Delta S^*$	$\Delta G^*$
1	1 <sup>st</sup>	0.99991	0.00	55.44	1.8 x10 <sup>8</sup>	52.4297	-0.21134	128.89
		0.99933	0.33	63.33	1.4x10 <sup>10</sup>	60.3278	-0.23293	144.61
		0.99886	0.50	67.72	3.2 x10 <sup>10</sup>	64.7113	-0.24496	153.34
		0.99833	0.66	72.04	7.8 x10 <sup>11</sup>	69.0364	-0.25685	161.97
		0.99696	1.00	81.89	3 x10 <sup>12</sup>	78.8774	-0.28398	181.63
		0.99195	2.00	115.9	3.5 x10 <sup>16</sup>	112.933	-0.37843	249.86
4	1 <sup>st</sup>	0.9878	0.00	130.64	5.6 x10 <sup>10</sup>	125.32	-0.24519	282.48
		0.97712	0.33	137.98	1.4 x10 <sup>11</sup>	132.65	-0.25659	297.13
		0.97024	0.50	141.87	6.9 x10 <sup>12</sup>	136.54	-0.26263	304.88
		0.96307	0.66	145.59	3.4 x10 <sup>12</sup>	140.26	-0.26843	312.32
		0.946651	1.00	153.72	7.4 x10 <sup>12</sup>	148.39	-0.28109	328.57
		0.907691	2.00	179.29	6.2 x10 <sup>14</sup>	173.96	-0.32107	379.77
6	1 <sup>st</sup>	0.95998	0.00	63.255	1.1 x10 <sup>7</sup>	59.5363	-0.19916	148.62
		0.98035	0.33	81.459	7.9 x10 <sup>10</sup>	77.7408	-0.23941	184.83
		0.98848	0.50	93.258	3.4 x10 <sup>10</sup>	89.5392	-0.26564	208.37
		0.99421	0.66	106.16	1.1 x10 <sup>13</sup>	102.444	-0.29443	234.15
		0.99985	1.00	140.15	1.2 x10 <sup>16</sup>	136.428	-0.37059	302.20
		0.986701	2.00	290.84	1.8 x10 <sup>36</sup>	287.123	-0.71136	605.33
10	1 <sup>st</sup>	0.97208	0.00	151.3	1.1 x10 <sup>18</sup>	148.2	-0.46505	317.1
		0.97634	0.33	165.8	8.6 x10 <sup>20</sup>	162.7	-0.505	346.1
		0.97837	0.50	173.7	6.2 x10 <sup>22</sup>	170.7	-0.52681	361.9
		0.98016	0.66	181.4	4.7 x10 <sup>23</sup>	178.4	-0.54813	377.4
		0.98364	1.00	198.7	1.5 x10 <sup>25</sup>	195.7	-0.59595	412.1
		0.99128	2.00	256.8	6.2 x10 <sup>38</sup>	253.8	-0.75652	528.4
16	1 <sup>st</sup>	0.9692	0.00	48.65	2.7 x10 <sup>6</sup>	43.58	-0.13592	126.54
		0.97459	0.33	57.66	4.9 x10 <sup>5</sup>	52.59	-0.15028	144.31
		0.97694	0.50	62.69	1.8 x10 <sup>5</sup>	57.62	-0.15837	154.29
		0.9793	0.66	67.69	6.9 x10 <sup>4</sup>	62.61	-0.16643	164.19
		0.98252	1.00	79.11	7.5 x10 <sup>5</sup>	74.03	-0.18500	186.95
		0.98951	2.00	119.12	2.7 x10 <sup>10</sup>	114.03	-0.25087	267.15

Order (n), Z (s<sup>-1</sup>), E\* (kJ mol<sup>-1</sup>),  $\Delta H^*$  (kJ mol<sup>-1</sup>),  $\Delta S^*$  (JK<sup>-1</sup> mol<sup>-1</sup>),  $\Delta G^*$  (kJ mol<sup>-1</sup>)

### X-ray powder diffraction

The X-ray powder diffraction patterns of five of the complexes namely **6**, **7**, **11**, **12** and **17** were recorded. The crystal lattice parameters were computed with the aid of the computer program TREOR. The observed 2 $\theta$  with relative intensity more than 10% are indexed and have been used for

evaluation. The crystal data (Table 6) of all the complexes fit well with the triclinic crystal system.

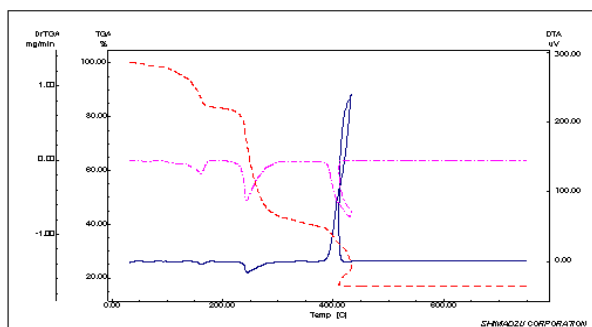


Fig. 6. TG-DTG curves of  $\{[\text{Co}(\text{pya})_2(\text{H}_2\text{O})_2]\cdot\text{H}_2\text{O}\}_n$  **1** in dynamic air.

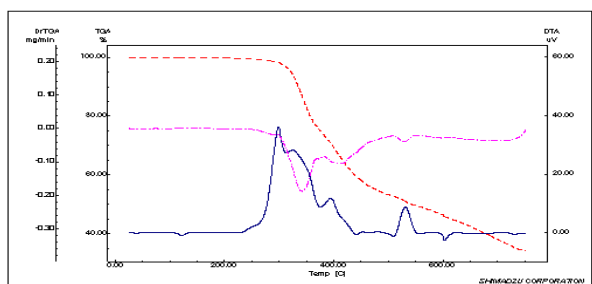


Fig. 7. TG-DTG curves of  $\{[\text{Cu}(\text{pya})_2(\text{dpm})]\cdot 0.5\text{H}_2\text{O}\}_n$  in dynamic air.

Table 6. Crystal data of the complexes.

Complex	6	7	11	12	17
a(Å)	5.64	8.78	6.79	8.19	5.54
b(Å)	10.02	7.77	8.54	8.93	9.29
c(Å)	8.72	16.97	14.23	15.83	15.68
α(d)	64.66	103.57	110.16	79.81	81.69
β(d)	112.15	57.91	74.83	63.62	102.92
γ(d)	135.91	105.24	70.38	72.02	102.34
Volume					
Unit cell(Å <sup>3</sup> )	308.59	937.07	663.37	985.51	764.21
Crystal system	triclinic	triclinic	triclinic	triclinic	triclinic

### Nano-sized particles of the metal coordination polymers

From the X-ray powder diffraction particle size of the complexes was calculated using the standard equation of Scherrer:

$$D = 0.94\lambda / \beta \cos\theta \quad (15)$$

where  $\lambda$  is the wavelength of the X-ray used,  $\beta$  is the full width at half maximum,  $D$  is the particle size and  $\theta$  is the angle between the incident and the scattered X-ray. The average crystallite sizes of the complexes were calculated to be in the range 15.7-19.6 nm (Table 7).

Table 7. Particle size of the complexes (nm)

Complex	6	7	11	12	17
particle size	15.7	19.6	14.8	18.1	18.7

### Catalytic activity of the coordination polymers

The analysis of the experimental data on the catalytic decomposition of  $\text{H}_2\text{O}_2$  by these complexes has been carried out. From the curves volume of oxygen evolved against time it is assumed that the decomposition reaction of  $\text{H}_2\text{O}_2$  is a zero order process. The rates of the reaction have been calculated according to:

$$V_t = V_0 + Kt \quad (16)$$

where  $V_t$  is the volume of oxygen evolved at time  $t$  (min),  $V_0$  is the volume of oxygen evolved before time measurements started (at  $t = 0$ ). Table 8 comprises the values of the specific rate constant  $k$  (in ml of oxygen per gram per min) of coordination polymers **1** and **17** under investigation that were computed from the corresponding  $V-t$  curves. One can observe that the data occurs at 5.61 and 4.53  $\text{ml}\cdot\text{min}^{-1}$ . In fact, the decomposition of  $\text{H}_2\text{O}_2$  requires the availability of interacting donor-acceptor sites on the coordination polymers. These sites can be established via intimately coupled pair of metal ions in different oxidation states. The transition metals may facilitate the exposure of such active sites [21].

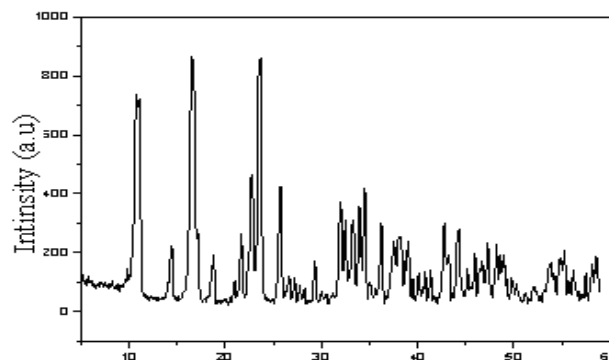


Fig. 8. Powder XRD pattern of **7**.

Table 8. The rate constant ( $k$ ,  $[\text{ml O}_2 \text{ min}^{-1}] (\text{g catalysts})^{-1}$ ) for  $\text{H}_2\text{O}_2$  decomposition on the indicated coordination polymers at 30°C (303K)

Complex	Rate constant, $k$ [ $\text{mL O}_2 \text{ min}^{-1}] (\text{g catalysts})^{-1}$ ]
$\{[\text{Co}(\text{pya})_2(\text{H}_2\text{O})_2]\cdot\text{H}_2\text{O}\}_n$ <b>1</b>	5.61
$\{[\text{Ni}(\text{pya})_2(\text{bzim})_2]\cdot 2\text{H}_2\text{O}\}_n$ <b>17</b>	4.35

### Microbiological Screening

Compounds **5**, **7** and **16** were tested their biological activity towards the following bacteria *Bacillus cereus* ( $G^{+ve}$ ), *Staphylococcus aureus* ( $G^{+ve}$ ), *Escherichia coli* ( $G^{-ve}$ ), *Pseudomonas aeruginosa* ( $G^{-ve}$ ), *Serratia marescens* ( $G^{-ve}$ ). The test revealed that compounds **7** and **16** exhibit antibacterial activity against both Gram positive (*Staphylococcus aureus* and *Bacillus cereus*) and Gram-negative strains (*Serratia marescens* and *Escherichia coli*). However, their activity was more pronounced against *E. coli* and Compound **5** inhibitory effect to *Bacillus cereus* (+ve).

The following fungi were also tested towards the three coordination polymers. These are *Aspergillus flavus*, *Candida albicans*, *Fusarium oxysporum*, *Geotrichum candidum*, *Scopulariopsis brevicaulis* and *Trichophyton rubrum*. The tests indicated that all fungi are resistant to the test compounds except for compound **7** that was active against *Aspergillus flavus* (Table 9).

It is to be noted that among the three studied coordination polymers compounds **7** and **16** are the most effective against bacteria and fungi. However compound **7** (the Ni(II) complex) is the only one that possesses antifungal activity presumably because benzimidazole is one of its constituents which exerts higher fungal activity as reported in the literature [22]. Furthermore, the three complexes exhibit variable antibacterial activities emphasizing the role of the metal ion nature and its coordination type on the normal cell process.

The lipophilic character of the metal center is greatly affected by coordination or chelation. In addition, compound **5** (the cobalt complex) could affect only the gram-positive *Bacillus cereus* while the other two were able to display antibacterial activity on both gram-negative (thin wall cell) and gram-positive (thick wall cell) bacteria [23].

**Table 9.** Antimicrobial activity of the coordination polymers.

Organisms	Samples No.		
	5	7	16
<i>Serratia marescens</i> (-ve)	0	12	13
<i>Pseudomonas aeruginosa</i> (-ve)	0	0	11
<i>Escherichia coli</i> (-ve)	0	20	18
<i>Staphylococcus aureus</i> (+ve)	0	15	15
<i>Bacillus cereus</i> (+ve)	11	14	14
Organisms	Samples No.		
	5	7	16
<i>Candida albicans</i>	0	0	0
<i>Geotrichum candidum</i>	0	11	0
<i>Fusarium oxysporum</i>	0	0	0
<i>Scopulariopsis brevicaulis</i>	0	0	0
<i>Trichophyton rubrum</i>	0	0	0
<i>Aspergillus flavus</i>	0	10	0

## 4. Conclusions

4-Pyridylacetic acid complexes provide a number of interesting structures. However, reports in the literature regarding mixed ligand metal complexes of this ligand are scarce. Therefore, we embarked on the preparation and characterization of certain mixed ligand complexes comprising a variety of auxiliary ligands that contain nitrogen and phosphorus binding sites. We think that our contribution will constitute together with the already prepared by other researchers a continuous set of complexes.

## Author Contributions

The following author contributions are indicated to be included in Credi taxonomy: The manuscript is a part of a Ph.D. thesis of Rasel Mukred. Aref A. M. Al and Asmaa I. El Said are supervisors.

Original: AAMA and AIE suggested the subject of the work, discussed the results and wrote the original draft and paper, RM performed the experiments and partly took part in the discussion. Revised: AAMA revised the thermal decomposition, X-ray diffraction, catalytic and biological activities as well as the references; AIE revised the spectroscopic methods as well as the check on the final version of the manuscript; RM revised the methodologies in the manuscript as well as tables and figures.

## References and Notes

- [1] a) Mautner, F. A.; Jantscher, P.; Fischer, R. C.; Torvisco, A.; Vicente, R.; Karsili, T. N.; Massoud, S. S. *Polyhedron* **2019**, *166*, 36. [Crossref] b) Sun, S.; Sun, Y.; Guo, H.; Fuo, X.; Guo, M.; Liu, S.; Guo, X.; Zhang, L.; Alexandrov, E. V. *Inorg. Chim. Acta* **2018**, *483*, 165. [Crossref]
- [2] Davarci, D. *Polyhedron* **2018**, *146*, 99. [Crossref]
- [3] Madalan, A. M.; Ene C D. *Inorg. Chim. Acta* **2018**, *475*, 184. [Crossref]
- [4] a) Aly, A. A. M.; Vatsadzeb, S. Z.; Walfort, B.; Reuffer, T.;

- Lang, H. *Russian J. Inorg. Chem.* **2017**, *62*, 1584. b) Louka, F. R.; Massoud, S. S.; Haq, T. M.; Koikawa, M.; Mikuriya, M.; Omote, M.; Fischer, R. C.; Mautner, F. A. *Polyhedron* **2017**, *138*, 177. [Crossref]
- [5] a) Twarog, K.; Holynska, M.; Kochel, A. J. *Inorg. Organomet. Polym. Mat.* **2018**, *28*, 548. b) Said, M. I.; El-Said, A. I.; Aly, A. A. M.; Abou-Taleb, A. *Ultrason. Sonochem.* **2018**, *46*, 68. [Crossref]
- [6] Li, J. X.; Hou, S. X.; Hao, C. G. H. *Transition Met. Chem.* **2017**, *42*, 661. [Crossref]
- [7] Li, X.; Cao, R.; Sun, Y. Q.; Shi, Q.; Yuan, D. Q.; Sun, D. F.; Bi, W. H.; Hong, M. C. *Cryst. Growth Des.* **2004**, *4*, 255. [Crossref]
- [8] Qin, Z.; Jennings, M. C.; Puddephatt, R. J.; Muir, K. W. *Inorg. Chem.* **2002**, *41*, 5174. [Crossref]
- [9] Geary, W. J. *Coord. Chem. Rev.* **1971**, *7*, 81. [Crossref]
- [10] Nakamoto, K. *Infrared and Raman Spectra of Inorganic and Coordination Compounds*. John Wiley & Sons, 6<sup>th</sup> edition, 2009. [Crossref]
- [11] Zhuang, J.; Zhao, D.; Luo, Z.; Yin, X.; Hao, H. *Synth. React. Inorg. Met. -Organ. Nano-Met. Chem.* **2011**, *41*, 1208. [Crossref]
- [12] Aly, A. A. M.; El-Said, A. I.; Gabr, R.; Mukred, R. A. *Am. Chem. Sci. J.* **2015**, *6*, 144. [Crossref]
- [13] Abu-Youssef, M. A. M.; Langer, V. *Polyhedron* **2006**, *25*, 1187. [Crossref]
- [14] Zidan, A. S. A.; Aly, A. A. M.; Ibrahim, G. H. H. *Assist. Uni. J. Chem. (AUJC)*, **2015**, *44*, 27.
- [15] Aly, A. A. M.; Gandour, M. A.; Al-Fakeh, M. S. *Turk. J. Chem.* **2012**, *36*, 69.
- [16] Zanguina, A.; Bayo-Bangoura, M.; Bayo, K.; Ouedraogo, G. V. *Bull. Chem. Soc. Ethiop.* **2002**, *16*, 73. [Crossref]
- [17] a) Aly, A. A. M.; Ghandour, A. M. S. *Turk. J. Chem.* **2012**, *36*, 69. b) Raman, N.; Raja, J. D.; Sakthivel, A. *Russ. J. Coord. Chem.* **2008**, *34*, 400. [Crossref] c) Lever, A. B. P. *Inorganic Electronic Spectroscopy*, 2nd edition, Elsevier, Amsterdam, 1984.
- [18] Coats, A. W.; Redfern, J. P. *Nature*, **1964**, *201*, 68. [Crossref]
- [19] Yusuff, K. K. M.; Karthikeyan, A. R. *Thermochim. Acta* **1992**, *207*, 193. [Crossref]
- [20] Chaudhary, R. G.; Ali, P.; Gandhare, N. V.; Tanna, J. A.; Juneja, H. D. *Arabian J. Chem.* **2019**, *12*, 1070. [Crossref]
- [21] Fahim, R. B.; Zaki, M. I.; Hussien, G. A. *Powder Technol.* **1982**, *33*, 161. [Crossref]
- [22] Zhou, Y.; Xu, J.; Zhu, Y.; Duan, Y. *Phytopathology* **2016**, *106*, 807. [Crossref]
- [23] Paison, F.; Su, B.; Pan, D.; Yan, T.; Wu, J. *Austin Biochem.* **2020**, *5*, 1025.

## How to cite this article

Aly, A. M.; El-Said, A. I.; Mukred, R. A. *Orbital: Electron. J. Chem.* **2020**, *13*, xx. DOI: <http://dx.doi.org/10.17807/orbital.v13i1.1551>